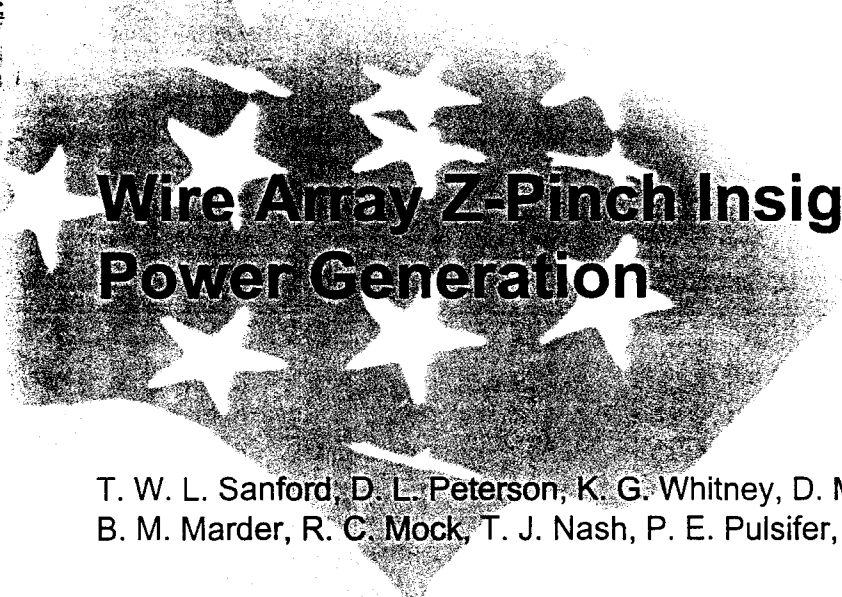


SANDIA REPORT

SAND97-3168

Unlimited Release

Printed August 1998



Wire Array Z-Pinch Insights for High X-Ray Power Generation

T. W. L. Sanford, D. L. Peterson, K. G. Whitney, D. Mosher, J. P. Apruzese, M. P. Desjarlais,
B. M. Marder, R. C. Mock, T. J. Nash, P. E. Pulsifer, and R. B. Spielman

Prepared by
Sandia National Laboratories
Albuquerque, New Mexico 87185 and Livermore, California 94550

Sandia is a multiprogram laboratory operated by Sandia Corporation,
a Lockheed Martin Company, for the United States Department of
Energy under Contract DE-AC04-94AL85000.

Approved for public release; further dissemination unlimited.



Sandia National Laboratories

Issued by Sandia National Laboratories, operated for the United States Department of Energy by Sandia Corporation.

NOTICE: This report was prepared as an account of work sponsored by an agency of the United States Government. Neither the United States Government, nor any agency thereof, nor any of their employees, nor any of their contractors, subcontractors, or their employees, make any warranty, express or implied, or assume any legal liability or responsibility for the accuracy, completeness, or usefulness of any information, apparatus, product, or process disclosed, or represent that its use would not infringe privately owned rights. Reference herein to any specific commercial product, process, or service by trade name, trademark, manufacturer, or otherwise, does not necessarily constitute or imply its endorsement, recommendation, or favoring by the United States Government, any agency thereof, or any of their contractors or subcontractors. The views and opinions expressed herein do not necessarily state or reflect those of the United States Government, any agency thereof, or any of their contractors.

Printed in the United States of America. This report has been reproduced directly from the best available copy.

Available to DOE and DOE contractors from
Office of Scientific and Technical Information
P.O. Box 62
Oak Ridge, TN 37831

Prices available from (615) 576-8401, FTS 626-8401

Available to the public from
National Technical Information Service
U.S. Department of Commerce
5285 Port Royal Rd
Springfield, VA 22161

NTIS price codes
Printed copy: A03
Microfiche copy: A01



SAND97-3168
Unlimited Release
Printed August 1998

Wire Array Z-Pinch Insights for High X-Ray Power Generation

T. W. L. Sanford*, **R. C. Mock**, and **T. J. Nash**
Diagnostics and Target Physics Department

M. P. Desjarlais and **B. M. Marder**
Target and Z-Pinch Theory Department

R. B. Spielman
Load Coupling and Z-Pinch Source Development Department

*Sandia National Laboratories**
P.O. Box 5800
Albuquerque, NM 87185-1196*

K. G. Whitney, **J. P. Apruzese**, and **P. E. Pulsifer**
*Naval Research Laboratory, Radiation Hydrodynamics Branch
Washington, DC 20375*

D. Mosher
*Naval Research Laboratory, Pulsed Power Physics Branch
Washington, DC 20375*

D. L. Peterson
*Los Alamos National Laboratory
Los Alamos, NM 87545*

ABSTRACT

Comparisons of detailed measured implosion characteristics of annular wire array z-pinchs with those modeled and simulated give insight into pinch dynamics and x-ray power generation.

*Invited paper presented at 12th International Conference on High-Power Particle Beams (Haifa, Israel, June 7-12, 1998)

ACKNOWLEDGMENTS

M. G. Haines (Imperial College) on his 1997 visit to Sandia, when he presented his Heuristic Model of the wire array z-pinch, rekindled our interest in understanding the basic mechanisms behind the measured power yield with wire number. We would like to thank him for many delightful and insightful discussions relating to both his and our research and for critiquing this paper. We thank also Y. Maron (Weizmann Institute) for the insight he provided during the early phases of this research, where he made the important suggestion that significant temperature gradients within the plasma are needed to explain the measured K-shell line ratios; C. Deeney for generously sharing his recent data on the implosions of 24-wires, which we have used in this paper; J. W. Thornhill (NRL) for his useful insights on the roll of shell thickness in influencing the plasma assembly dynamics; the late G. O. Allshouse, J. S. DeGroot (UCD), D. A. Hammer (Cornell), J. H. Hammer (LLNL), M. K. Matzen, R. B. Spielman, K. W. Struve, W. A. Stygar, A. Toor (LLNL), and F. J. Wessel (UCI) for useful technical discussions; G. A. Chandler, D. L. Fehl, T. L. Gilliland, D. O. Jobe, J. S. McGurn, J. F. Seamen, K. W. Struve, W. A. Stygar, M. F. Vargas and the Saturn and Z crews for their dedicated technical support; and W. Beezhold, D. L. Cook, G. Cooperstein (NRL), J. Davis (NRL), M. E. Jones (LANL), R. J. Leeper, J. E. Maenchen, M. K. Matzen, D. H. McDaniel, J. P. Quintenz, J. J. Ramirez, and G. Yonas for their vigorous programmatic support that has made this research possible.

Contents

INTRODUCTION	1
RESULTS AND DISCUSSION	1
CONCLUSION	16
REFERENCES	17

Figures

1. (A) Peak total radiated power (solid line) and pulsewidth (estimated using XRD filtered by 1- μ m kimfol [dashed line]), (B) Radial convergence, (C) Total radiated energy normalized by calculated kinetic energy assuming a 10:1 convergence, (D) Ion number density (K-shell region), and (E) Electron temperature (K-shell region) versus gap. 2	
2. Normalized pulseshape in three energy channels for two gaps.....	3
3. Calculated ion density and electron temperature for aluminum Z shot.....	5
4. Rise-time and effective pulsewidth versus gap.....	8
5. Measured total radiated power pulsewidth (estimated using XRD filtered by 5- μ m kimfol) and KART model versus gap.....	9
6. (A) Measured, modeled (KART), and simulated (E-RMHC) total radiated power pulsewidth (estimated using XRD filtered by 5- μ m kimfol) and (B) measured and simulated peak total radiated power versus mass.	13
7. A) Measured, modeled (KART), and simulated (E-RMHC) total radiated power pulsewidth (estimated using XRD filtered by 5- μ m kimfol) and (B) measured and simulated peak total radiated power versus radius.	14
8. E-RMHC simulated energy partition	15

INTRODUCTION

The discovery [1] that the use of very large numbers of wires enables high x-ray power to be generated from wire-array z-pinchs represents a breakthrough in load design for large pulsed power generators, and has permitted high temperatures to be generated in radiation cavities [2-5] on Saturn [6] and Z [7]. In this paper, changes in x-ray emission characteristics as a function of wire number, array mass, and load radius, for 20-mm-long aluminum arrays on Saturn that led to these breakthrough hohlraum results, are discussed and compared with a few related emission characteristics of high-wire-number aluminum and tungsten arrays on Z. X-ray measurement comparisons with analytic models and 2-D radiation-magnetohydrodynamic (RMHC) code simulations in the x-y [8] and r-z [9] planes provide confidence in the ability of the models and codes to predict future x-ray performance with very-large-number wire arrays.

RESULTS AND DISCUSSION

Wire Number Variation: In the first set of Saturn aluminum wire-number experiments [1], the array mass was fixed and the wire number was varied by more than an order of magnitude from 10 to almost 200 by simultaneously changing the interwire gap and the wire size. This procedure was carried out for a 0.62-mg and a 0.84-mg array having an initial radius of 8.6 mm and 12 mm, respectively. The variation permitted interwire gaps to be explored from 6 mm down to 0.4 mm for both the small- and large-radius arrays. Decreasing the interwire gap resulted in monotonic decreases in the rise-time and width of the x-ray pulse and simultaneous increases in radiated power and energy, in the *same way for both array radii* (Figure 1). Over the 6 to 0.4 mm gap reduction explored, the total radiated power increased by a factor of 20 (Figure 1A) and the total radiated energy by a factor of 2 (Figure 1C).

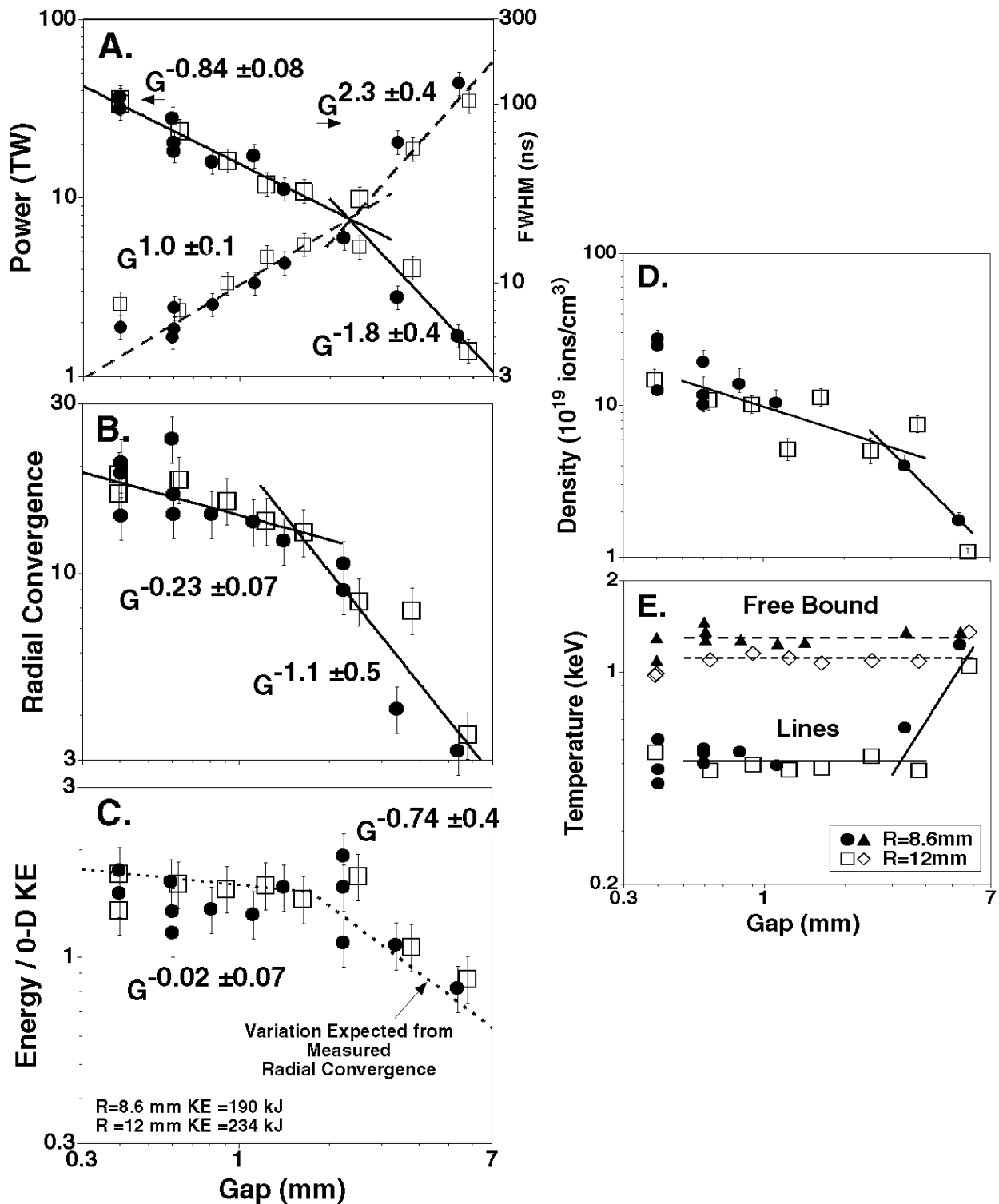


Figure 1. (A) Peak total radiated power (solid line) and pulsewidth (estimated using XRD filtered by 1- μm kimfol [dashed line]), (B) Radial convergence, (C) Total radiated energy normalized by calculated kinetic energy assuming a 10:1 convergence, (D) Ion number density (K-shell region), and (E) Electron temperature (K-shell region) versus gap.

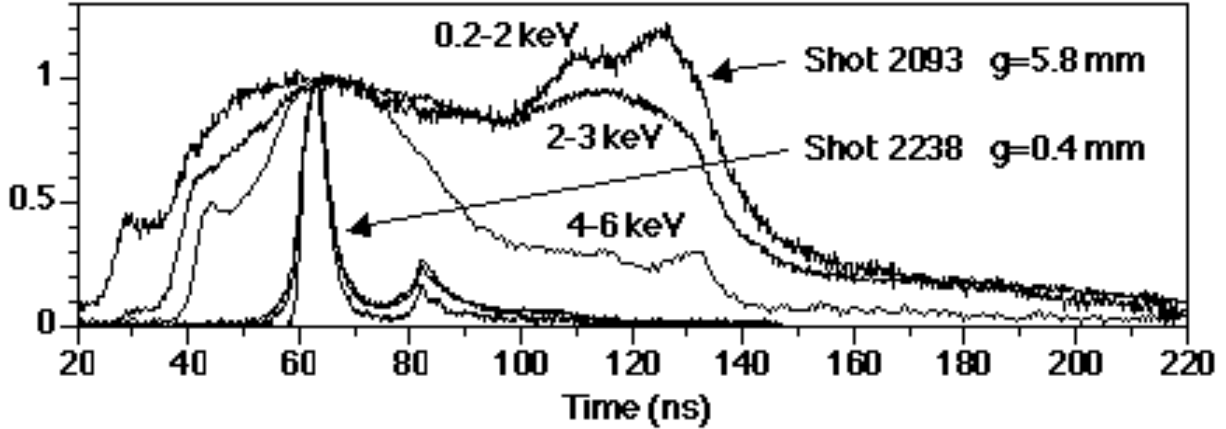


Figure 2. Normalized pulseshape in three energy channels for two gaps.

In addition, for gaps smaller than 2 ± 0.6 mm, the character of the x-ray emission qualitatively changed, transitioning from a broad, single, irregular radiation pulse at large gaps, to a strong, narrow, evenly-shaped radiation pulse, that was followed by a much weaker pulse at small gaps (Figure 2). The weaker pulse is consistent with a second radial implosion [10]. For gaps greater than ~ 2 mm, time-integrated images of the pinch exhibit the presence of a kink ($m=1$) as well as a sausage ($m=0$) instability; time-dependent images show significant precursor plasma stagnating on axis, generating soft x-ray emission tens of nanoseconds prior to the main implosion, in agreement with earlier [11] and current [12] experiments. For gaps less than ~ 2 mm, on the other hand, no kink instability is observed, with only a minimal precursor plasma forming. Moreover, the change in the temporal shape of the x-ray pulse (Figure 2) and spatial quality of the pinch occurred with corresponding quantitative transitions in the rates of change as a function of gap of (1) the emitted total x-ray power (Figure 1A), (2) the average size of the K-shell emission region (Figure 1B), (3) the emitted total x-ray energy (Figure 1C), (4) the average K-shell emitting ion density (Figure 1D), and (5) electron temperature (Figure 1E). The emitting ion densities and electron temperatures were inferred from x-ray size data together with the K-shell power and K-series spectrum data. Not enough data were taken at wide gap spacings, however, to ascertain how rapidly this transition in x-ray behavior took place. For this reason, we represent it experimentally as a transition between two power laws as illustrated in Figure 1, with the power indicated by the dependence on gap (G) shown in Figure 1. The Heuristic Model developed by Haines [13] also

shows a sharp change of behavior at this critical gap, representing whether merger of the exploding single wires occurs early on or during the implosion. In the latter case, inward jetting of plasma and the accumulation on axis of a plasma column can change the phenomenology.

Measurement of the slope of the optically-thin, free-to-bound, x-ray emission (Figure 1E) determines the electron temperature of the hot core of the pinch [10]. It exhibits no variation with gap (dashed lines) and is only a function of the implosion kinematics. For large gaps, where the measured ion density at stagnation is low, the temperature extracted from K-shell line ratios [14] (solid lines) agrees with that extracted from the free-to-bound emission. At these low densities, the ion-electron equipartition rate could be the dominating process, giving a slower rate of rise of x-ray emission [20]. As the gap decreases and the emitting ion density increases (Figure 1D), however, the optical depth of the K-shell emission becomes significant, and the line ratio begins to reflect the temperature of the outside surface of the emitting region, rather than an average over the region. This transition from a thin to a thick plasma, as indicated by the data of Figure 1E, approximately coincides with the transition in the rate of change of density with gap (Figure 1D) and with the transition at ~ 2 mm.

The difference between the core and surface temperature is indicative of a substantial temperature gradient within the emitting plasma. The enhanced plasma density at small gaps increases the temperature and density gradients and opacity effects, but in such a way as to approximately maintain the average amount of mass participating in the K-shell emission at $\sim 11\%$, independent of gap [15]. Comparisons of the measured K-shell emission radii with that simulated by the Eulerian-RMHC (E-RMHC) [9] indicate that the actual mass averaged radius is about double that extracted from the emission images [16]. This gradient structure is illustrated by a detailed analysis [17] of the x-ray image, spectral, and K-shell power data, for an aluminum-array shot taken on Z, having an interwire gap of 0.5 mm, a total mass of 4.1 mg, and an array radius of 20 mm. The density and temperature profiles obtained from a best fit of an aluminum-plasma collisional-radiative-equilibrium model to these measured quantities is shown in Figure 3. In the model, the radiative transfer is carried out for all optically-thick K-shell lines and two K-shell continual temperatures.

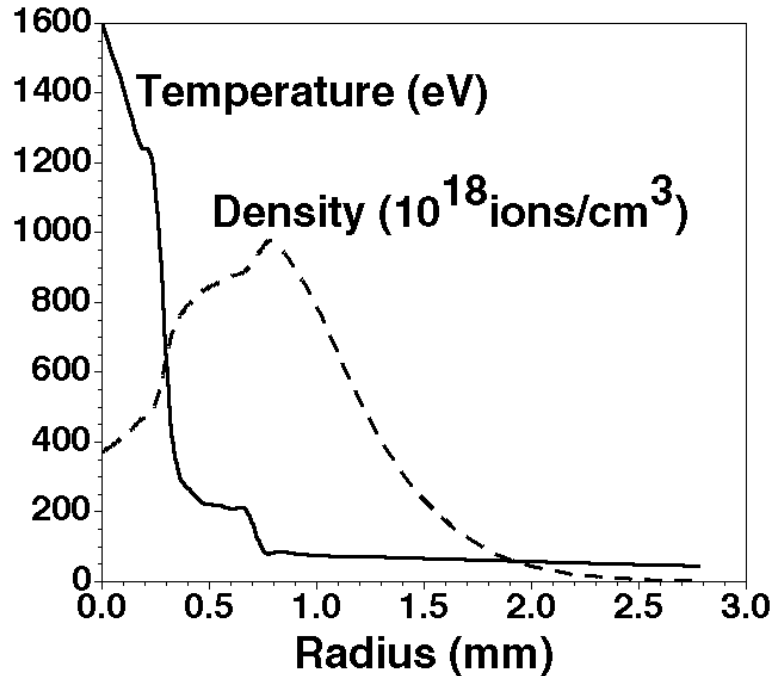


Figure 3. Calculated ion density and electron temperature for aluminum Z shot.

Interpretation of Number Variation: In general, variations in peak total power track the inverse of the measured pulsewidths (Figure 1A), as would be expected if the total energy radiated during stagnation is slowly varying. The greater rate of dependence with gap of the pulsewidth relative to the peak power, for gaps greater than ~ 2 mm reflects the greater disorganization of the implosion as seen by the lost double-pulse nature of the stagnation (Figure 2). The accelerated rate of decrease in power for large gaps relative to that for small gaps is consistent with the decrease in total radiated energy (Figures 1A, 1C, and 4). This change in energy is approximately consistent with the change in the calculated kinetic energy (dotted lines in Figure 1C calculated from the experimental radial convergence (Fig. 1B)), and by inference, the radiated energy. Importantly, the trends in ion density (Figure 1D) and electron temperature (Figure 1E) demonstrate that the *increase in power is the result of systematically greater plasma compression and not the result of an increase in temperature.*

The apparent transition in implosion quality near 2 mm has been interpreted using an RMHC in x-y geometry [1, 8]. Calculations performed with this code show (in correspondence

with the experimental data) that a change in the implosion topology occurs with increasing wire number. The implosion is seen to make a transition from one composed of non-merging, self-pinching, individual wire plasmas to one characterized by the early formation and subsequent implosion of a quasi-plasma-shell, as also found in the Heuristic Model. The shell had density and current variations distributed azimuthally that were correlated with the initial wire location and which decreased in amplitude with decreasing gap. The calculated transition region was sensitive to (1) the magnitude of the prepulse that accompanies the main current pulse, (2) the current flowing per wire, (3) the wire size, (4) the interwire gap, and (5) the resistivity model used. For the particular resistivity model used and for the measured prepulse and wire sizes used, this transition was found to occur between wire numbers 20 to 80 (or between interwire gaps of about 3 to 1 mm, respectively) for the small radius load [1]. This calculated transition was also seen to be consistent with observations made with 1.3-mm gap loads in the transition region. There, individual wires were observed to neck-off in the form of bright spots (similar to Beg et al. [18]) 20 ns prior to peak radiated power (where the array had only imploded a fraction of a mm radially). Ten nanoseconds later, after the array had imploded an additional 1.5 mm, the observed plasma emission became a continuous distribution, with no evidence of individual wire structure. Here, we refer to the small wire-number region where $g > 2$ mm as the “wire-plasma” regime, and the large wire-number region where $g < 2$ mm as the “plasma-shell” regime.

The x-y simulations [8] together with analytic modeling [19] show that the wire-plasmas (in contrast to the plasma of a shell) accrue azimuthal velocity components during the implosion owing to (1) deviations in the locations of the individual wires from those of a perfect annulus, or (2) to wire-to-wire current nonuniformities, or (3) to the presence of the limited number of current return posts surrounding the array [19], which could seed higher number instabilities.

These velocity components produce density asymmetries at stagnation that can contribute to the reduction in both the compressibility of the stagnating plasma and the resulting radiated energy, both in qualitative agreement with the discontinuity observed in the radial convergence measurements (Figure 1B) and in the energy channel (Figure 1C). The x-y simulations show, however, that these variations *cannot* account for the change in measured pulse shape for any wire number greater than 10. The finite electron-ion-energy equipartition time is probably dominant here [20]. In contrast, E-RMHC [9] simulations in the r-z plane, which assume an azimuthally symmetric plasma shell with a random density distribution in the r-z direction, suggest that the shape of the primary power pulse and the general change in peak power with gap are related to the evolution of the thickness of the plasma sheath due to r-z motions and the growth of Rayleigh-Taylor (RT) instabilities. This thickness is calculated to scale linearly with the pulsewidth [15]. The measured *rise-time* of the total radiation pulse *and* the “*effective*” *pulsewidth* (defined as the total energy divided by the peak power) *scale as the gap*, over the entire gap range explored, showing no discontinuity near 2 mm (Figure 4). This data, together with the simulations, thus suggest a direct relation between the initial interwire gap and the resulting thickness of the imploding sheath. This relation is in agreement with the Heuristic Model, since the expansion velocity of each wire is almost invariant [18, 20].

Other experimental data [18], however, show the evolution of inward plasma jetting from each wire plasma, decreasing with wire number [21], that leads to a prepinch plasma on axis and thus to a softer final pinch when stagnation of the entire array occurs. In addition, as is included in the Heuristic Model, the larger final radius of the pinch leads to a slower equipartition of energy from ions to electrons and to a slower development of the x-ray power. These many processes thus suggest that *the simple scaling with gap discussed here is likely masking several complex processes*.

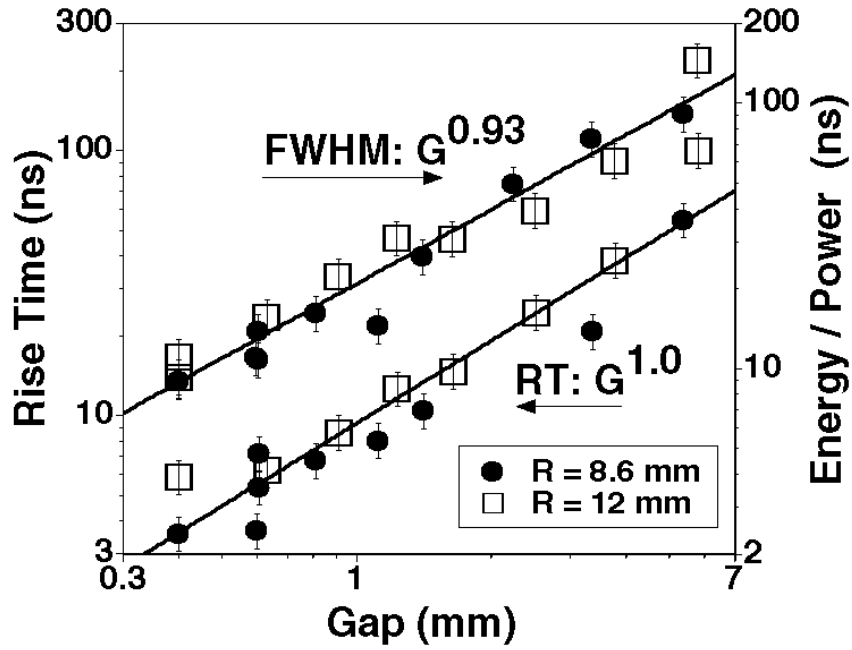


Figure 4. Rise-time and effective pulsewidth versus gap

Wire-Array Modeling: Though the RMHC computations can reproduce many features of the radiation dependence on gap, they do so by imposing an arbitrary initial density-perturbation amplitude on a fixed-thickness annular plasma. This amplitude is varied empirically for each interwire gap to best fit the experimental radiation characteristics. However, the physical mechanisms for the dependence of radiation performance on gap remain unresolved. X-Y simulations, particularly with appropriate atomic physics included [20], can model aspects of the merging, jetting, axial accretion, equipartition times, and the experimental azimuthal asymmetries. But since it appears that the final radius is strongly influenced by RT instabilities in the r-z plane, it seems important that 3-D codes are implemented.

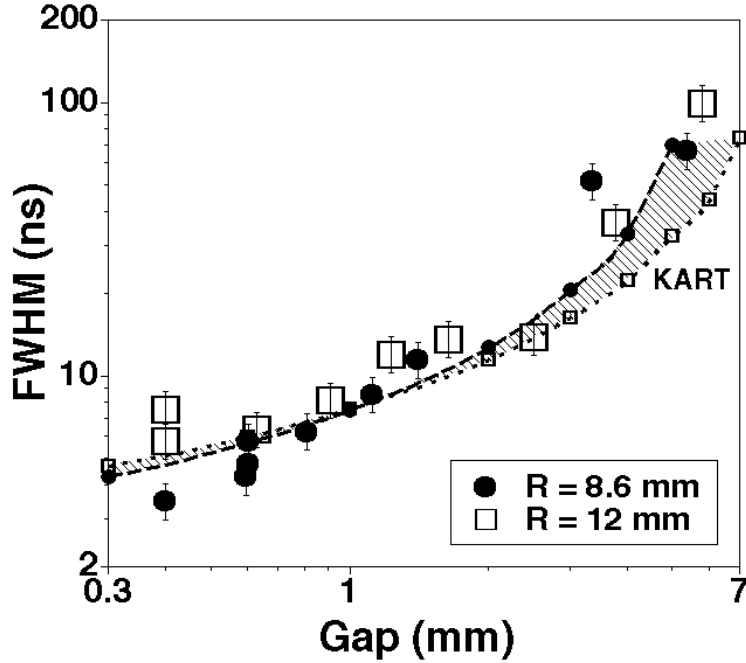


Figure 5. Measured total radiated power pulsewidth (estimated using XRD filtered by 5- μm kimfol) and KART model versus gap.

Recently, a fundamentally 3-D analytic model (KART) of the implosion has been developed by Desjarlais and Marder [22] that takes into account an amplification of the RT instability arising from a kink instability, which deforms the individual wire plasmas. This deformation is in phase with that generated by the RT instability, which is assumed to arise from a global sausage instability acting on the entire array. The agreement of their estimated pulsewidth (as illustrated in Fig. 5) with the measured pulsewidths of Fig. 1A, as well as with that measured for other tungsten experiments on Saturn [23] and Z [7, 24], with only *one perturbation parameter that scales with the wire size*, suggests that the wires retain enough of their individual identity for a sufficient time to allow amplification of the RT instability from the kink instability to participate. Doubling the number of tungsten wires on Z from 120 to 240, for example, reduced the measured pulsewidth by $(29 \pm 9)\%$ [24], in agreement with a calculated 25% reduction.

For the plasma-shell regime, a number of intrinsically three-dimensional mechanisms have been proposed that consider how expansion dynamics of the individual wire-plasmas and

their subsequent merging into plasma annuli create perturbations that disrupt the plasma during implosion. The Heuristic Model for perturbations in the plasma annulus produced by the merging of arrays of fine wires is based on the development of MHD sausage modes during the expansion phase of individual wires observed in Imperial College experiments and modeled in 2-D [18, 25]. The model is based, in part, on the following assumptions. Sausage modes in individual wires grow until the plasmas of adjacent wires merge, after which current flow in a continuous plasma annulus stops their growth. Wire-to-wire sausage perturbations are uncorrelated. At the merging time, the mean radius of the individual wire plasma is half of the inter-wire gap, so that the thickness of the annulus at merging is given by the gap. A statistical average in perturbed line density over all the wires in the array is then used to determine the initial annular perturbation. Analytic estimates are then made of its effect on the development of RT instabilities during implosion of the annulus and subsequent x-radiation characteristics. The dependence of implosion quality on gap enters (1) in the thickness of the initial annulus and a reduced average perturbation amplitude for larger wire numbers, (2) in the degree of radial plasma jetting, and (3) in an effect estimated for long equipartition times. The dominant wavelength of the RT is found at stagnation.

A second model for the plasma-shell regime is also based in part the above assumptions for wire-expansion dynamics, but makes different assumptions for the wavelength of the perturbations in the annulus formed by the merged wires [26]. Recent observations of the development of short-axial-wavelength plasma flares around the expanding wire-plasma cores [27] have been combined with the Imperial College observations and analyses [18, 25] to supplement the above picture. The sausage perturbations growing on the expanding wire plasmas are nonlinear and large-amplitude even at very-early times in their development. The shapes of

the perturbation is self-similar in the radial scale, that is, they “look” the same independent of radius. The observed bifurcations in expanding single-wire plasmas [18, 25] follow directly from the self-similar assumption. Thus, the fundamental (longest) wavelength in the perturbation spectrum grows as the wire plasma expands, so that at the merging time, both the thickness of the annulus and the dominant perturbation wavelength are comparable to the interwire gap. For this self-similar model, the amplitude of the initial perturbation is always large, while its wavelength scales with gap. The gap dependence of implosion quality and radiated pulse width then derives from larger gaps (smaller wire numbers) producing longer-wavelength perturbations that are more disruptive during implosion of the annulus.

Though this process is intrinsically 3-D in nature, 2-D E-RMHC [9] simulations can help to determine if the gap dependence of initial annular thickness and perturbation wavelength established by the self-similar model can reproduce the observed dependence of radiation characteristics without resorting to an arbitrarily-chosen perturbation amplitude. However, the model does provide for RT saturation and healing for sufficiently-short wavelength (small gap/large wire number). Also, the E-RMHC simulations show that tripling the scale of 10% and 15% initial perturbations is equivalent to perturbations of 45% and 75% at the shorter-scale, demonstrating that perturbation wavelength is a powerful determining factor for implosion quality and radiation pulse width.

Mass and Radius Variation: Two sets of additional Saturn aluminum-wire experiments were conducted in the calculated high-wire-number, quasi-plasma-shell regime [16]. These experiments show two important trends. First, when the mass of the 12-mm-diameter arrays (which used 192 wires) is reduced from above 1.9 to below 1.3 mg, a factor of two decrease in pulsewidth (Figure 6A), with an associated doubling of the peak total radiated power, (Figure 6B) occurs [28]. Second, when the array radius is increased from 8.6 to 20 mm, for a mass of 0.6 mg in 136 wires, the total radiated pulsewidth (Figure 7A) increases from only ~4 to ~7 ns and the associated peak total radiated power (Figure 7B) remains relatively unchanged with radius [29].

Interpretation of Mass and Radius Variation: The E-RMHC [9] simulations were used to understand the underlying pinch dynamics of these variations [20, 21]. Over the mass range of 0.42 to 3.4 mg and radius range 8.6 to 20 mm measured, which spanned an implosion time of 40 to 90 ns, the implosion time of the simulated pulse agrees with that measured within a shot-to-shot variation of only 2 ns. This agreement suggests that $(100 \pm 7)\%$ of the initial mass is being accelerated during the implosion. For these simulations, the electron-photon coupling was set to either its nominal value (indicated by N) or a reduced value (indicated by R), such that the calculated peak total radiated power agreed with that measured at ~ 0.6 mg (Fig. 6B). Within the uncertainty of this emissivity approximation, the measured pulsewidth (Figures 6 and 7) and trends in total radiated peak power agree with that simulated, using only a *single value* of a density perturbation seed. KART calculations are also shown in Figures 6A and 7A.

For all cases, the E-RMHC simulations show a *two-stage* development of the instability with initial bubble burst when a wavelength of the order of the shell thickness is reached, followed immediately by current flow in the low-density material between the spikes. The plasma shell self-heals and continues to accelerate with only a small amount of bubble material being thrown ahead of the main body of plasma. The instability growth continues, evolving to longer wavelengths, until one of the order of the new shell thickness is reached. When the shell bursts the second time (at longer wavelengths), a significant amount of material is accelerated to the axis, and the radiation pulse begins. These simulations show that the decrease in pulsewidth and associated doubling of the peak total power, as mass is reduced, is due to the faster implosion velocity of the plasma shell relative to the growth of the shell thickness. The relative increase in peak power for the higher-energy x-rays is due to an increase in ion temperature, arising from an increase in kinetic energy per incident ion at stagnation. The simulations also show that the increase in pulsewidth with radius is due to the faster growth of the shell thickness relative to the increase in shell velocity. These results suggest that the improved uniformity provided by the large number of wires in the initial array reduces the disruptive effects of instabilities observed in small-wire-number imploding loads.

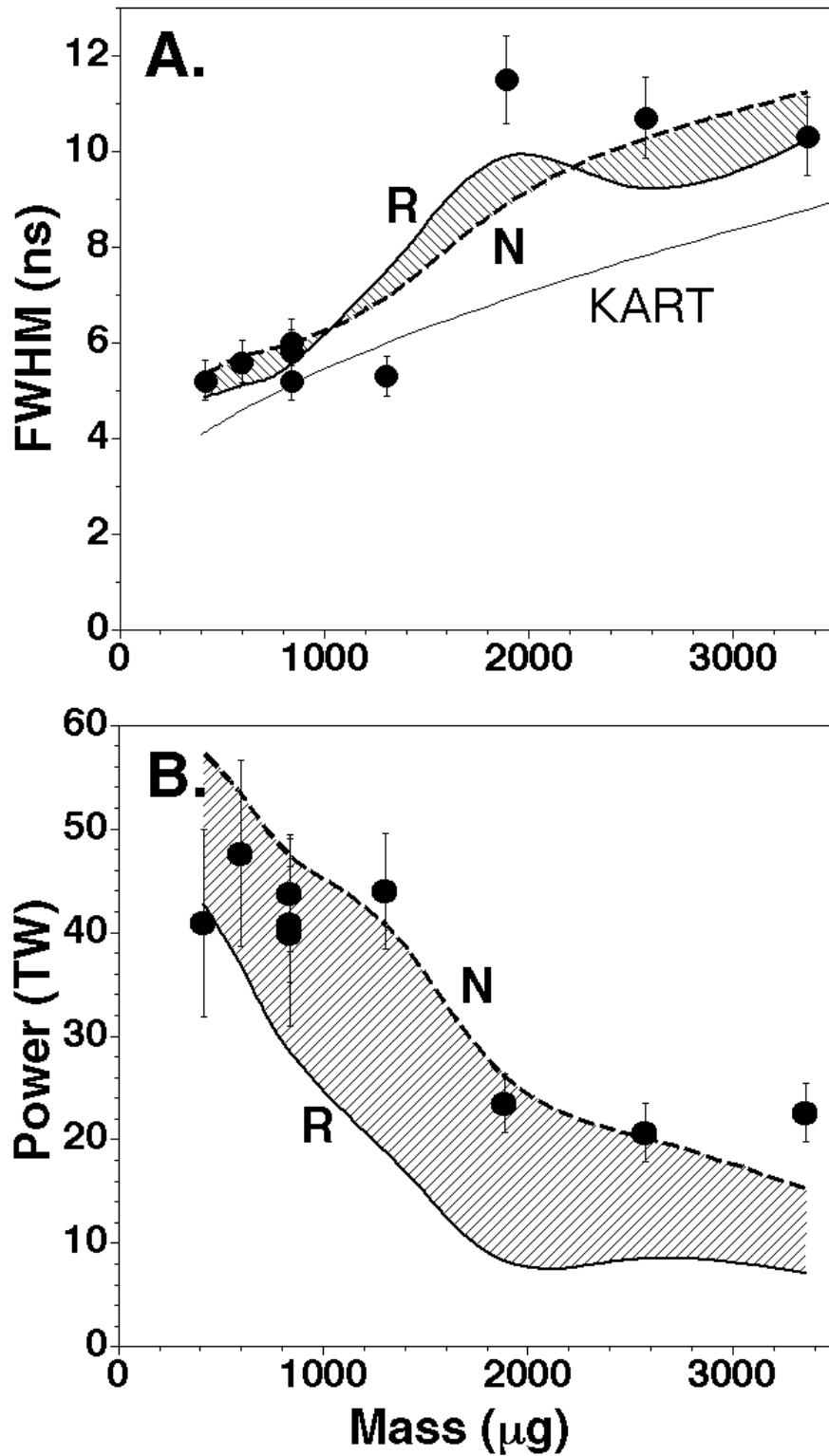


Figure 6. (A) Measured, modeled (KART), and simulated (E-RMHC) total radiated power pulsewidth (estimated using XRD filtered by 5- μm kimfol) and (B) measured and simulated peak total radiated power versus mass.

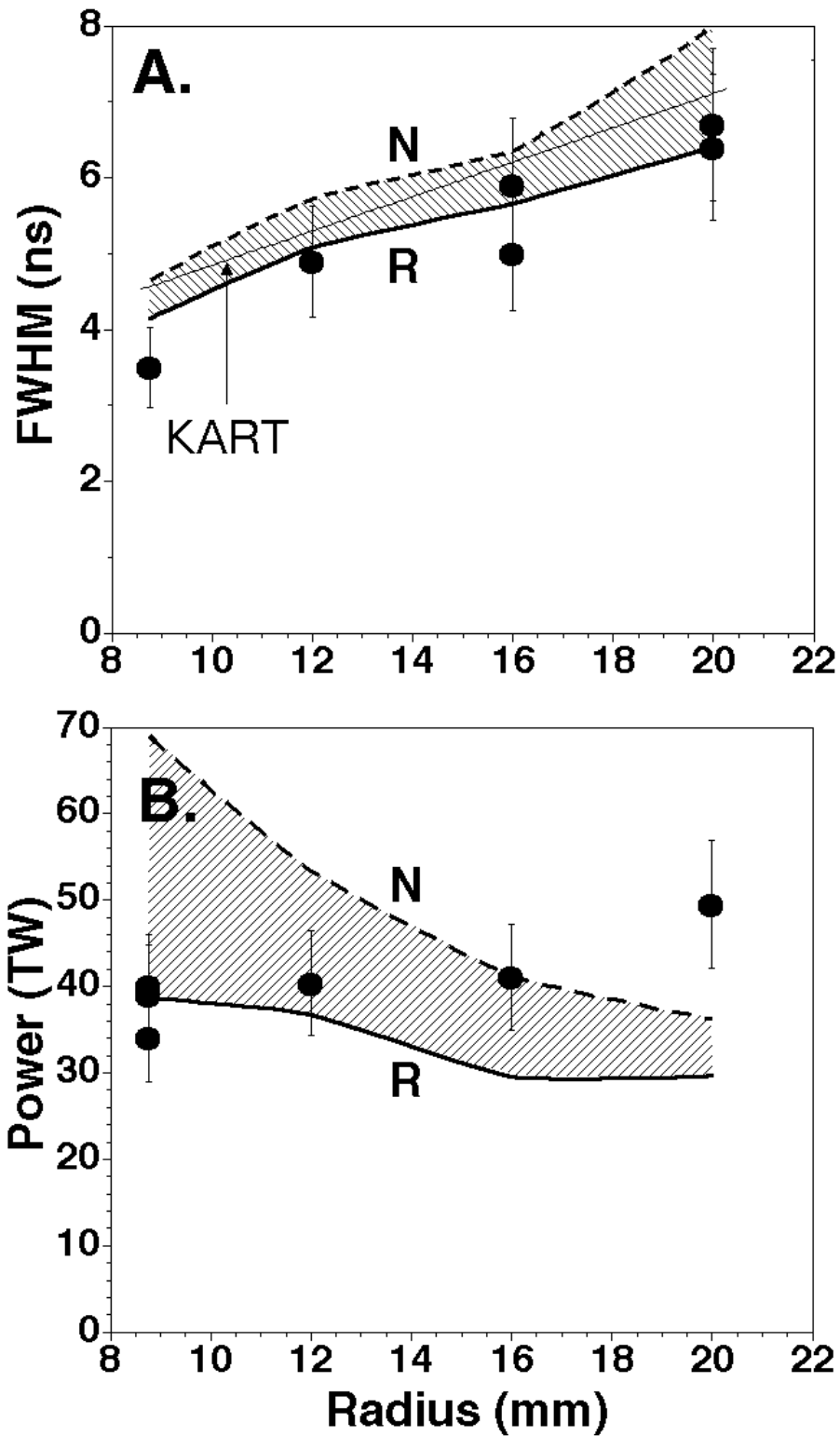


Figure 7. A) Measured, modeled (KART), and simulated (E-RMHC) total radiated power pulsewidth (estimated using XRD filtered by 5- μ m kimfol) and (B) measured and simulated peak total radiated power versus radius.

The simulations generate total radiation pulse shapes in agreement with the primary pulse measured, as illustrated in Figure 8, for a 0.84-mg, 12-mm radius, 192-wire-number load. The simulations indicate that the energy deposited in the plasma arises primarily from the Lorentz ($\mathbf{J} \times \mathbf{B}$) force and goes primarily into accelerating the plasma, increasing its kinetic energy. At early times when instabilities have not become important and there has been little plasma heating, the simulated energy deposited by the Lorentz force and the plasma radial kinetic energies are nearly equal. At later times, the instability destroys the plasma shell, accelerating plasma to the axis where it stagnates, and the kinetic energy diverges from the work generated by the Lorentz force. The plasma that has not stagnated continues to be accelerated by the Lorentz force. Because the radiation rate is higher than the rate at which energy is being supplied, the total kinetic energy decreases, even though some plasma continues to be accelerated. As the pressure rises, some of the ($\mathbf{J} \times \mathbf{B}$) energy is transferred to internal energy by $p dV$ work, rather than as a kinetic-energy increase. Due to the extended radial nature of the plasma as stagnation begins, the

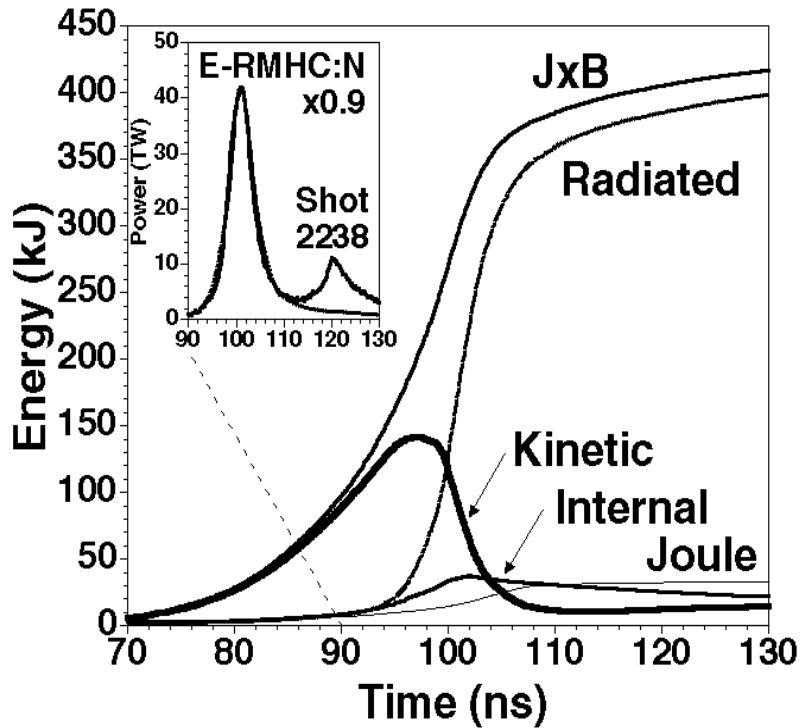


Figure 8. E-RMHC simulated energy partition

net result on the energy flow is that part of the plasma on axis releases energy as radiation, while regions away from the axis continue to absorb energy, which may then be radiated later in the pulse. The result is a total radiated energy that is higher than the instantaneous peak in the kinetic energy at the time stagnation begins. The calculations show only a small contribution from Joule heating.

The variation with mass on Z using tungsten wires in the high-wire-number regime shows similar trends to those observed on Saturn for the aluminum wires [7, 24]. On Z, the pulsewidth decreased by a factor of two and the total radiated power doubled when the mass decreased from 6 to 4 mg, for loads having a 20-mm radius, with 120-wire-number. Moreover, these high-wire-number implosions, with interwire gap of 0.5 mm, produced high-quality implosions that had pulsewidths of only ~ 7 ns near peak power.

CONCLUSION

Implosions that develop narrow pulsewidths with high peak powers can be generated from both small- and large-radius annular wire arrays by keeping the interwire gap to spacings on the order of 0.5 mm or less. Reducing the implosion time, while still providing good current coupling to the load at stagnation, reduces the growth of the radial instabilities relative to the implosion velocity and permits the highest powers to be developed. The E-RMHC simulations [9], the Heuristic Model [13], and the KART model [22] agree with aspects of the data and provide insight into the underlying dynamics. A new self-similar model [26] for the initial E-RMHC perturbation dependence on gap provides additional insight and may improve that codes predictive capability for future large-wire-number experiments on Z.

REFERENCES

- [1] T. W. L. Sanford, et al., *BEAMS'96*, pp. 146-149; *Phys. Rev. Lett.* **77**, 5063 (1996).
- [2] M. K. Matzen, *Phys. Plasmas* **4**, 1519 (1997).
- [3] J. P. Quintenz, et al., this conference.
- [4] D. L. Cook, this conference.
- [5] G. Yonas, this conference.
- [6] D. D. Bloomquist, et al., *Proc. 6th Int. IEEE Pulsed Power Conf.*, (1987), p. 310.
- [7] R. B. Spielman, et al., *BEAMS'96*, pp. 150-153; *Phys. Plasmas* **5**, 2105 (1998).
- [8] B. M. Marder, et al., to be published *Phys. Plasmas* (Aug. 1998).
- [9] D. L. Peterson, et al., *Phys. Plasmas* **3**, 368 (1996).
- [10] T. W. L. Sanford, et al., *Phys. Plasmas* **4**, 2188 (1997).
- [11] C. Deeney et al., *Phy. Rev. E* **51**, 4823 (1995).
- [12] S. V. Lebedev, et al. "Azimuthal Structure and Global Instability In the Implosion Phase of Wire Array Z-Pinch Experiments" submitted to *Phys. Rev. Lett.* (1998).
- [13] M. G. Haines "Heuristic Model of the Wire-Array Z-pinch", to be published in *IEEE Trans on Plasma Sci: Special Z-Pinch Edition A* (Aug. 1998).
- [14] K. G. Whitney, et al., *Phys. Rev. E* **56**, 3540, (1997).
- [15] T. W. L. Sanford, "Systematic Trends in X-Ray Emission Characteristics of Variable-Wire-Number, Fixed-Mass, Aluminum-Array, Z-Pinch Implosions", submitted to *Phys. Plasmas* (Aug. 1998).
- [16] T. W. L. Sanford, et al., *Dense Z-Pinches 4th Int. Conf.*, AIP (1997), pp. 561-573.
- [17] J. P. Apruzese, et al., submitted to *Phys. Plasmas* (Aug. 1998).
- [18] F. N. Beg, et al., *Plasma Phys. And Controlled Fusion*, **39**, 1-25 (1997).
- [19] D. Mosher, *BEAMS'94*, pp. 159-162.
- [20] M. G. Haines, private communication.
- [21] S. V. Lebedev, et al., "Azimuthal Structure and Global Instability In the Implosion Phase of Wire Array Z-Pinch Experiments" submitted to *Phys. Rev. Lett.* (June 1998).

- [22] B. M. Marder and M. P. Desjarlais, *IEEE Conference Record Abstracts, 1998 International Conference on Plasma Science, (Raleigh, North Carolina, June 1-4,1998)*, IEEE Catalog Number 98CH36221, 268 (1998).
- [23] C. Deeney, et al., *Phys. Rev. E* **56**, 5945 (1997).
- [24] T. W. L. Sanford, et al., “Wire Number Doubling in High-Wire-Number Regime Increases Z-Accelerator X-Ray Power”, to be published in *IEEE Trans on Plasma Sci: Special Z-Pinch Edition A* (Aug. 1998).
- [25] J.P. Chittenden, et al., *Bull. Am. Phys. Soc.* **41**, 1471 (1996).
- [26] D. Mosher, et al., “Modeling Initial Annular Perturbations in Large Wire-Number Arrays,” work in progress.
- [27] D. Mosher, et al., “Plasma Evolution in Linear Arrays of Tungsten Wires during Prepulse”, work in preparation.
- [28] T. W. L. Sanford, et al., “Increased X-Ray Power Generated from Low-Mass Large-Number Aluminum-Wire-Array Z-Pinch Implosions”, to be published in *Phys. Plasmas* (Oct. 1998).
- [29] T. W. L. Sanford, et al., “Symmetric Aluminum-Wire Arrays Generate High-Quality Z-Pinches at Large Array Radii”, to be published in *Phys. Plasmas* (Oct. 1998).

**Sandia is a multiprogram laboratory operated by the Sandia Corp., a Lockheed Martin Co., for the US DOE under Contract DE-AC04-94AL85000.

DISTRIBUTION

- | | | | |
|----|--|----|--|
| 3 | University of New Mexico
Dept. of Chemistry & Nuclear Eng.
Attn: Prof. G. Cooper
Prof. S. Humphries
Prof. N. F. Roderick
Albuquerque, NM 87131 | 1 | University of California Davis
Attn: Prof. John deGroot
Department of Applied Science
228 Walker Hall
Davis, CA 95616 |
| 10 | Los Alamos National Laboratory
Attn: R. J. Macek
R. Stringfield
H. A. Thiessen
R. J. Faehl
D. L. Peterson (5 copies)
W. Matuska
R. Bowers
P. O. Box 1663
Los Alamos, NM 87545 | 23 | Naval Research Laboratory
Attn: G. Cooperstein
D. Hinshelwood
D. Mosher (5 copies)
J. M. Neri
P. Ottinger
F. C. Young
R. Commisso
J. Davis
K. G. Whitney (5 copies)
J. P. Apruzese
P. E. Pulsifer
J. L. Giuliani
W. Thornhill
Washington, DC 20375 |
| 2 | Mission Research Corporation
Attn: D. R. Welch
K. Struve
1720 Randolph Road SE
Albuquerque, NM 87106 | 1 | Columbia University
Physics Department
Attn: Prof. W. Lee
538 W. 120 Street
New York, NY 10027 |
| 1 | Titan Industries
Attn: R. B. Miller
P. O. Box 9254
Albuquerque, NM 87119 | 2 | Cornell University
Laboratory of Plasma Sciences
Attn: Prof. J. B. Greenly
Prof. D. A. Hammer
369 Upson Hall
Ithaca, NY 14853-7501 |
| 5 | Fermilab
Attn: Prof. L. M. Lederman,
Director Emeritus
J. H. Christenson
H. B. Jensen
T. E. Nash
M. Month
P. O. Box 500
Batavia, IL 60510 | | |

1	Massachusetts Institute of Technology Plasma Fusion Center Attn: Prof. R. D. Petrasso 167 Albany St. Cambridge, MA 01239	4	Pulse Science Inc. Attn: V. Bailey I. Smith J. Fockler P. Spence 600 McCormick St. San Leandro, CA 94577
1	New York University Physics Department Attn: Prof. J. Sculli 4 Washington Place New York, NY 10003	7	Lawrence Livermore National Laboratory Attn: P. T. Springer A. Toor M. D. Rosen M. Tabak J. H. Hammer G. B. Zimmerman R. S. Thoe P. O. Box 808 Livermore, CA 94550
1	University of Maryland Laboratory for Plasma and Fusion Energy Studies Attn: Prof. M. Reiser College Park, MD 20742		
3	Imperial College Blackett Laboratory Attn: Prof. M. G. Haines J. P. Chittenden F. N. Beg London SW7 2BZ ENGLAND	2	Atomic Weapons Research Establishment Attn: P. Thompson J. C. Martin Aldermaston, Reading RG7 4PR Berkshire ENGLAND
2	Berkeley Research Associates Attn: N. R. Pereira J. Golden P. O. Box 852 Springfield, VA 22150	1	Culham Laboratory Culham Lightning Studies Unit Attn: C. J. Hardwick Abingdon, Oxfordshire OX14 3DB ENGLAND
6	Physics International Co. Attn: H. Helava J. Creedon C. Gilman Sik-Lam Wong J. C. Riordan P. Sincerny 2700 Merced Street San Leandro, CA 94577	3	Rutherford Appleton Laboratory Attn: T. G. Walker, Director of Research and Development P. Sharp, Director of Technology T. Broome Chilton, Didcot Oxon. OX11 0Qx ENGLAND
		1	Weizmann Institute Department of Nuclear Physics

	Attn: Prof. Y. Maron	1 MS 1181	Jim Asay, 9511
	Rehovot 76100 ISRAEL	1 MS 1182	Doug Bloomquist, 9530
3	Kernforschungszentrum Karlsruhe	1 MS 1182	Tim J. Renk, 9514
	GmbH.	1 MS 1182	Steven L. Shope, 9514
	Attn: W. Bauer	1 MS 1185	Bob Turman, 9514
	H. Bluhm	1 MS 1185	Mark Kiefer, 9542
	P. Hoppe	1 MS 1185	Paul L. Mix, 9542
	Postfach 3640, D-7500 Karlsruhe 1	1 MS 1186	David B. Seidel, 9542
	FEDERAL REPUBLIC OF	1 MS 1186	Michael Cunio, 9574
	GERMANY	1 MS 1186	M. P. Desjarlais, 9574
		1 MS 1186	Melissa R. Douglas, 9574
		1 MS 1186	Thomas Hail, 9574
6	C. E. R. N.	1 MS 1186	David Hanson, 9574
	CH-1211	1 MS 1186	Joel S. Lash, 9574
	Attn: W. Blum	1 MS 1186	Barry M. Marder, 9574
	V. Chabaud	1 MS 1186	Eugene J. McGuire, 9574
	G. Jarlskog	1 MS 1186	Tom Mehlhorn, 9574
	G. Lutz	1 MS 1186	Stephen A. Slutz, 9574
	W. Manner	1 MS 1186	Roger Vesey, 9574
	P. Weilhammer	1 MS 1186	Dale R. Welch, 9574
	Geneva 23	1 MS 1187	Keven Baker, 9573
	SWITZERLAND	1 MS 1187	T. L. Gilliland, 9573
		1 MS 1187	Michael J. Hurst, 9573
1	MS 0151 Gerry Yonas, 9000	1 MS 1187	Dan Jobe, 9573
1	MS 1106 Arthur W. Sharpe, 9342	1 MS 1187	Keith Matzen, 9570
1	MS 1107 K. Mikkelson, 9342-1	1 MS 1187	John McKenney, 9573
1	MS 1152 Larry X. Schneider, 9543	1 MS 1187	John L. Porter, 9570
1	MS 1153 M. T. Buttram, 9330	1 MS 1187	Larry E. Ruggles, 9573
1	MS 1153 M. Collins Clark, 9331	1 MS 1187	Johann F. Seamen, 9573
1	MS 1153 Dale Coleman, 9331	1 MS 1187	Walter W. Simpson, 9573
1	MS 1155 Wendland Beezhold, 9300	1 MS 1187	Mark Vargas, 9573
1	MS 1159 M. A. Hardemann, 9344	1 MS 1188	Richard G. Adams, 9512
1	MS 1165 Joe Polito, 9300	1 MS 1188	Dave Bliss, 9512
1	MS 1165 Larry D. Posey, 9300	1 MS 1188	Stewart Cameron, 9512
1	MS 1167 E. Fred Hartman, 9343	1 MS 1188	Roy Hamil, 9512
1	MS 1170 Juan Ramirez, 9580	1 MS 1188	Craig Olson, 9500
1	MS 1170 Gary Rochau, 9580	1 MS 1191	Jeff Quintenz, 9502
1	MS 1170 G. A. Zawadzkas, 9302	1 MS 1193	Dean Rovang, 9515
1	MS 1178 Paul Raglin, 9581	1 MS 1193	John Maenchen, 9515
1	MS 1179 William P. Ballard, 9341	1 MS 1193	M. G. Mazarakis, 9515
1	MS 1179 David E. Beutler, 9340	1 MS 1194	Dillon McDaniel, 9540
1	MS 1179 John A. Halbleib, 9341	1 MS 1193	Peter Menge, 9515
1	MS 1179 Ronald P. Kensek, 9341	1 MS 1194	J. Frank Camacho, 9544
1	MS 1179 J. R. Lee, 9340	1 MS 1194	Chris Deeney, 9544
1	MS 1179 L. J. Lorence, 9341	1 MS 1194	S. E. Rosenthal, 9544

5 MS 1194 Rick Spielman, 9544
1 MS 1194 Ken Struve, 9544
1 MS 1194 William A. Stygar, 9544
1 MS 1196 Thomas E. Alberts, 9577
1 MS 1196 G. A. Chandler, 9577
1 MS 1196 Mark S. Derzon, 9577
1 MS 1196 David L. Fehl, 9577
1 MS 1196 Dave Hebron, 9577
1 MS 1196 Ray J. Leeper, 9577
1 MS 1196 Anne R. Moats, 9577
1 MS 1196 Raymond C. Mock, 9577
1 MS 1196 Tom J. Nash, 9577
1 MS 1196 Richard E. Olson, 9577
1 MS 1196 Carlos L. Ruiz, 9577
15 MS 1196 Thomas W. L. Sanford,
9577
1 MS 1196 Al Schmidlapp, 9577
1 MS 1196 Michael A. Stark, 9577
1 MS 1196 Jose A. Torres, 9577
2 MS 0899 Technical Library, 4916
1 MS 0619 Print Media, 12615
1 MS 9018 CTF, 8940-2
2 MS 0619 Review and Approval
Desk, 12690
For DOE/OSTI